PAPER • OPEN ACCESS

Production of negatively charged radioactive ion beams

To cite this article: Y Liu *et al* 2017 *New J. Phys.* **19** 085005

View the article online for updates and enhancements.

New Journal of Physics

The open access journal at the forefront of physics

CrossMark

OPEN ACCESS

PAPER

Production of negatively charged radioactive ion beams[*]

Y Liu[1,3] , **D W Stracener**[1] **and T Stora**[2]

1   Physics Division, Oak Ridge National Laboratory, Oak Ridge, TN 37831, United States of America
2   ISOLDE, CERN, CH-1211 Geneva 23, Switzerland
3   Author to whom any correspondence should be addressed.

E-mail: liuy@ornl.gov

Abstract

Beams of short-lived radioactive nuclei are needed for frontier experimental research in nuclear structure, reactions, and astrophysics. Negatively charged radioactive ion beams have unique advantages and allow for the use of a tandem accelerator for post-acceleration, which can provide the highest beam quality and continuously variable energies. Negative ion beams can be obtained with high intensity and some unique beam purification techniques based on differences in electronegativity and chemical reactivity can be used to provide beams with high purity. This article describes the production of negative radioactive ion beams at the former holifield radioactive ion beam facility at Oak Ridge National Laboratory and at the CERN ISOLDE facility with emphasis on the development of the negative ion sources employed at these two facilities.

1. Introduction

The study of radioactive nuclei far from stability is at the very frontier of nuclear science [1, 2]. Research with these exotic nuclei addresses a wide range of important topics in fundamental nuclear science, including the underlying nature and stability of atomic nuclei, the origin of elements, the evolution of the cosmos, and tests of current models for the fundamental interactions that are basic to the structure of matter. It also provides the scientific foundation for innovative applications for society such as discovering new radionuclides for cancer diagnosis and treatment, detecting nuclear contraband at ports of entry, and assessing the safety of our nuclear stockpile. The experimental research in this frontier relies heavily on the range and intensity of radioactive ion beams (RIBs) available in the laboratory, which has provided the impetus for worldwide construction of RIB facilities dedicated to providing beams of short-lived nuclei for fundamental and applied research. A number of reviews summarize the recent progress in upgrading the capabilities of existing RIB facilities and constructing next-generation RIB facilities throughout the world [3–6].

Two complementary methods of RIB production are commonly used: in-flight fragmentation [6, 7] and isotope separator on-line (ISOL) [8, 9]. The in-flight method is based on a heavy ion beam, accelerated to high energies to bombard a relatively thin production target. Interaction of the beam particles with the target nuclei results in a wide range of radioactive nuclei via projectile fragmentation and in-flight fission. A system of large-acceptance dipole magnets then separate out the rare isotopes of interest for use in experiments. In the ISOL approach, a light ion beam (typically protons, deuterons, or helium isotopes) from a driver accelerator strikes a thick production target producing radioactive nuclei via nuclear reactions. The target material is kept at high temperature, enabling the radioactive species to diffuse out of the target and subsequently effuse to an ion source to be ionized, extracted, and accelerated to a mass separator where the beam of interest is selected. A post-accelerator is often needed to further accelerate the radioactive ions to desired energies for experiments. The in-

flight method requires one high-energy, heavy-ion accelerator and, since the process is independent of chemistry, it is universal and fast. The fragment ions are produced and separated at velocities similar to that of the primary beam, so rare isotopes with half-lives down to microseconds can be obtained. However, if the radioactive ions need to be slowed down for the particular experiment, the resulting beams have large emittance and large energy spread. In contrast, the ISOL method relies on diffusion and effusion processes in the target and ion source, and the associated delay times make beams of short-lived isotopes (<1 s) much more difficult to produce, especially for refractory and chemically reactive elements. However, with post-extraction acceleration, the ISOL technique can be used to provide intense RIBs with excellent beam quality and well defined and variable energies that are required for detailed studies in nuclear structure and nuclear astrophysics. Because of these unique research opportunities, a number of RIB facilities are based on the ISOL technique [4, 10–13].

The ion sources used at ISOL facilities are compact and are designed for high efficiency for specific elements, with the ability to ionize trace quantities of radioisotopes in a high background of other elements [14, 15]. While ion sources for stable elements generally focus on production of high ion currents, ion sources for RIB generation focus on selectivity and efficiency due to the often extremely low production rates of the radioactive isotopes of interest. Furthermore, compact and rugged designs capable of stable operation over a few weeks in harsh radiological and thermal environments are required. In most facilities, positive-ion beams are used either at low energies directly from the ion source or injected into an accelerator such as a linac or a cyclotron. Negative ion generation is of particular importance for RIB facilities employing tandem electrostatic accelerators for post-acceleration, owing to the fact that these accelerators require negative-ion injection. Beams from a tandem accelerator have precisely controlled energies, good energy resolution, and excellent beam quality (low emittance and small beam size) and, hence, are ideally suited to study reactions of fundamental importance in nuclear physics and nuclear astrophysics. A particular example is the capability to search for resonances in reaction cross-sections relevant to explosive nucleosynthesis in astrophysical systems such as novae, supernovae, and x-ray bursts [16]. This unique capability has led to the construction of a few ISOL facilities designed with a tandem as the post-accelerator [8] including the former HRIBF at ORNL [12].

Venezia and Amiel [17] first demonstrated the production and separation of negative ions of radioactive iodine isotopes from fission products by surface ionization and electromagnetic separation at the Soreq on-line isotope separator. In their initial work, the graphite catcher for fission fragments acted as the surface ionizer and the yields of negative iodine ions were very low. One of the reasons for the low ion yields was the relatively high work function of the graphite. A negative surface ionization source with low work function material LaB_6 as the ionizer was later developed [18] and used to study the fission yields of short-lived bromine and iodine isotopes [19]. Low yields of negative radioactive ions of Br and I were also obtained from a UO_2-graphite surface [20] for delayed neutron emission studies at the SOLAR on-line mass spectrometer facility [21].

The first on-line production of intense negative RIBs of halogens [14, 22] was obtained with an efficient negative surface ionization source at the ISOLDE RIB facility for research in solid state and nuclear physics [23, 24]. The ion source was equipped with a planar sintered porous LaB_6 ionizer and demonstrated 10%–50% ionization efficiencies for Cl, Br, I and At. A similar LaB_6 ionizer configuration was employed in a source to provide halogen isotopes for nuclear spectroscopy at the on-line mass separator OSTIS [25]. The early experiments at ISOLDE revealed that the LaB_6 ionizer was susceptible to poisoning when it was used with inappropriate target materials decomposing at high temperatures. Since then, some progress has been made in mitigating the drawbacks and improving the performance of the ISOLDE negative surface ionization source by various means, including new ionizer geometries, new low work function ionizer materials, and proper choice of target materials [24, 26]. Recently at ORNL (in early 2016) an ion source with a LaB_6 ionizer was used for several weeks to provide pure beams of radioactive bromine and iodine for studies of total decay heat in fission products and for measurements of the production rate of antineutrinos in the decay of fission fragments.

The former HRIBF used a 25 MV tandem for post-acceleration with the unique capability to accelerate RIBs to energies above the Coulomb barrier for nuclear physics experiments [12]. Both positive-ion and negative-ion sources were developed or adapted at HRIBF for this research program. Although negative RIBs were commonly produced by charge exchange in a Cs-vapor cell to convert initially positive ion beams to negative ion beams prior to injection into the tandem accelerator, negative ion generation with a negative ion source was preferred for some RIBs. In spite of the limitation in ion-species capability, negative ion sources offer distinct advantages to perform research activities with RIBs [14]. For example, direct production of negative ions eliminates the charge exchange process to transform positive ions into negative ions, which is generally inefficient and often results in a rather large, undesired energy spread in the resulting negative beams due to multiple scattering of the ions in the charge exchange cell volume (see section 2). Since, in many cases, the purity of the RIB is crucial to the success of the experiment, selectivity in the ion source can be very useful. Negative surface ionization sources are highly selective—only the elements with high electron affinities can be efficiently ionized. This property has been used to great advantage to obtain high purity negative RIBs for certain elements, such as the halogens, for which the positively charged counterparts are often contaminated by isobars from neighboring elements and

Table 1. Measured charge exchange efficiencies with Cs-vapor (unpublished data from HRIBF) for selected elements.

Element	EA (eV)	Conversion efficiency (%)	Beam energy (keV)
As	0.81	42	20
		30.7	40
Se	2.02	22	20
		16.6	40
Sn	1.22	41	50
Br	3.37	0.6	20
		0.8	40
		1.2	50
Sr	0.05	0.6	20
		0.9	40
Rb	0.498	0.5	50

Note. Column 2 lists the electron affinity (EA) of the element. Column 3 gives the measured efficiency for conversion into negative ions for the specific positive-ion beam energy shown in Column 4.

molecular sidebands. For these reasons, extensive research effort has been devoted to the development of negative ion sources for specific RIBs of interest [12, 14].

The present paper describes the research and development that has been conducted at the former HRIBF and the ISOLDE facility for the production and purification of negative RIBs for fundamental and applied research. Section 2 provides brief descriptions of the methods of negative ion formation with emphasis on the specific ion source techniques employed for negative RIB production at these two facilities. Section 3 provides a review of negative RIB production at the former HRIBF. Section 4 presents the specific negative ion sources developed at HRIBF and ISOLDE as well as the latest results of negative RIB production at ISOLDE. Section 5 discusses beam purification methods based on negative ions. Finally, future developments and new concepts for the production of negative RIBs are discussed in section 6.

2. Methods of negative ion formation

Negative ions can be produced by double charge-exchange of positive ions produced with a positive ion source or by direct extraction from a negative ion source. For the production of negative RIBs, charge-exchange has been the most frequently used method. The charge-exchange process is considered to be a two-step process in which positive ions sequentially capture two electrons as they interact with a vapor target of low ionization potential (IP) metal, such as Cs or Na. The yield of negative ions depends on the collision energy (beam energy), the electron affinity (EA) of the projectile element, the IP of the target element, and the density of the exchange vapor. In general, highest yields are expected for the projectile-target combinations with minimum energy defects in both of the electron-capture processes [27–31]. Table 1 lists the charge-exchange efficiencies measured at the HRIBF for some elements with a Cs-vapor charge-exchange cell (CEC). As noted, the highest efficiencies for producing As^- (EA = 0.81 eV), Sn^- (EA = 1.22 eV), and Se^- (EA = 2.02 eV) are respectively, 42%, 41%, and 22%, with optimum projectile energies ranging from 20 keV to 50 keV, while the best efficiency for Br^- (EA = 3.37 eV) beams was only 1.2%. Extensive studies of negative ion formation by charge transfer in metal vapors have been reported [30]. These studies show optimal conversion efficiencies of ~0.5 to >90% for various elements considered. In particular, Heinemeier *et al* reported 2%–6% efficiencies for elements with very low EA values, such as Be^- (EA = 0.24 eV, metastable), B^- (EA = 0.28 eV) and Fe^- (EA = 0.25 eV) using Na or Mg vapors and a fixed projectile energy of 20 keV. These results indicate that useful intensities of negative RIBs can be obtained for many elements with a proper selection of the charge exchange vapor and the ion energy.

Although positive ion sources in combination with a CEC is a versatile means of generating negative RIBs, as pointed out earlier, negative ion sources are desired for certain radioactive species for higher beam intensities and better beam purity. The major challenge associated with radioactive beam production at an ISOL facility concerns the required fast release and efficient ionization of radioactive trace products from the target-and-ion-source unit within a much larger vapor load of impurities from the target and structural materials. Consequently, the ion source should ideally exhibit high efficiency, high temperature operation, simple design, radiation resistance, and long lifetime. Although a variety of negative ion sources are available, a limited number of them can meet these criteria. The most successful and widely employed for RIB applications has been negative-ion sources based on surface ionization. Sputter-type negative ion sources have also been used for some

specific beams such as fluorine and for isotopes with relatively long lifetimes. The basic principles of these negative ion sources are discussed below, while the detailed descriptions of the specific sources are given in section 4.

2.1. Negative surface ionization

When neutral atoms or molecules come into the proximity of a hot metal surface, a certain fraction of them will be thermally desorbed as positively or negatively charged ions, depending on the electropositive or electronegative nature of the neutral species. The underlying physics and theory of this surface ionization process have been extensively studied and reviewed [32–34] and will not be described in detail here. Briefly, for the formation of negative ions, under thermodynamic equilibrium conditions, the degree α of ionization for neutral particles of EA E_a evaporating from an ideal surface with a work function ϕ at temperature T is quantitatively given by the Saha–Langmuir equation:

$$\alpha = \frac{n_i}{n_0} = \frac{g_i}{g_0} \exp\left(\frac{E_a - \phi}{k_B T}\right), \tag{1}$$

where n_i and n_0 are the numbers of the ions and neutrals respectively leaving the surface in unit time, g_i and g_0 are the statistical weights of the ionic and neutral states, respectively, and k_B is the Boltzmann constant. The ionization efficiency β is defined as the ratio of the negative ion flux leaving the surface to the incident neutral flux and is given by

$$\beta = \frac{\alpha}{1 + \alpha} = \left[1 + \frac{g_0}{g_i} \exp\left(\frac{\phi - E_a}{k_B T}\right)\right]^{-1}. \tag{2}$$

These equations show that for high ionization efficiencies $E_a > \phi$ is required. If $E_a - \phi > k_B T$, the negative ion formation process is exothermic and $\beta \sim 1$. This requirement could be met for high EA elements such as halogens. In fact, negative surface ionization has been a preferred method for halogen RIBs because of the high efficiency and high purity due to low ionization efficiency for neighboring elements, such as noble gases and alkali metals.

LaB$_6$ has a low work function in the range of 2.4–3.0 eV [35, 36] and has been most frequently used as the ionizer material for generating negative halogen beams. Since the majority of the elements in the periodic table have electron affinities less than the work function of LaB$_6$, it cannot provide good negative ion yields for most elements. In addition, LaB$_6$ is known to dissociate and evaporate at temperatures of about 1400 °C under vacuum and is prone to poisoning from impurities outgassing from the target material. Therefore, it is extremely desirable to find materials with lower work functions that can maintain their properties at high temperature with variable impurity loads. New ionizer materials have been investigated [26] at ISOLDE, including gadolinium hexaborides ($\phi = 1.5$ eV), alloys of iridium and cerium ($\phi = 2.6$ eV), and tungsten impregnated with low work function oxides such as BaO and SrO ($\phi = 1.0$ eV). It is well known that the work function of a metal surface can be lowered by adsorption of minute amounts of low work function materials such as the alkali metals. This approach was also explored [37] in a source equipped with a permeable Ir ionizer and controlled feeding of a highly electropositive vapor such as Cs through the Ir matrix to decrease the surface work function for negative ion generation.

Equation (2) gives the surface ionization efficiency for a planar surface. For a tubular (cavity) geometry, provided that the neutral isotopes have the possibility to interact several times with the cavity material and have a high probability to be captured in the plasma well before extraction, significantly higher efficiencies for all halogens are predicted. The enhancement is expressed as N in a modified Saha–Langmuir expression in equation (3) [38]:

$$\beta = \frac{N\alpha}{1 + N\alpha} = \left[1 + N\frac{g_0}{g_i} \exp\left(\frac{\phi - E_a}{k_B T}\right)\right]^{-1}. \tag{3}$$

The theoretical Saha–Langmuir ionization efficiencies for planar and tubular LaB$_6$ ionizer configurations are reported for some representative parameters in figure 1, reflecting the two types of ion sources that have been operated online at ISOLDE with pulsed proton beam from the PSBooster [26]. The variation in the effective work function of LaB$_6$ surface, from a nominal value of 2.6–2.9, and 3.4 eV, reflects the possible variations of the material properties and poisoning by impurities in the target-ion source unit and has a strong influence on the predicted efficiencies. As shown for Astatine this variation can lead up to a 500-fold change in the ionization efficiency. In contrast, a variation of 200 K of the LaB$_6$ surface temperature will minimally affect the efficiencies if the work function is constant. For a planar ion source (MK4), the maximum achievable ionization efficiency of 50% comes from a geometrical 'view' factor of the ion source configuration-about 50% probability for the isotopes to escape the target-ion source unit without interaction with the LaB$_6$ ionizer. A high efficiency is predicted for cavities with work functions of 2.6 eV, e.g., approaching 100% for halogens, and reasonable efficiencies are obtained even when poisoning is observed to degrade the work function of the LaB$_6$ ionizer up to
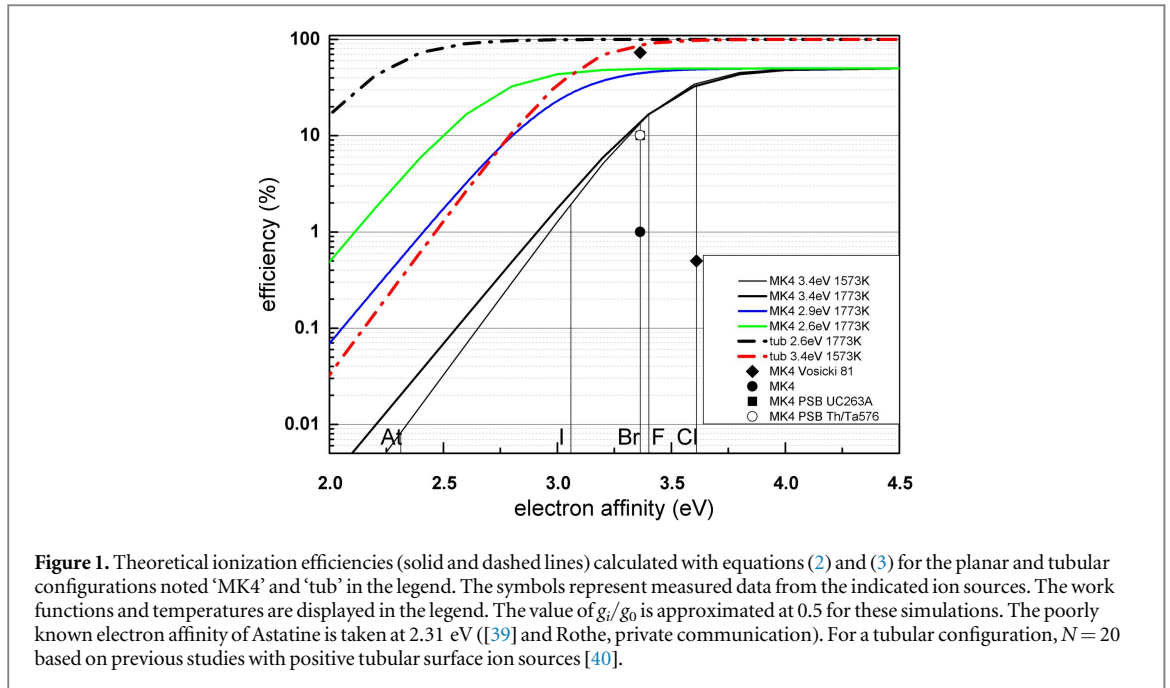
Figure 1. Theoretical ionization efficiencies (solid and dashed lines) calculated with equations (2) and (3) for the planar and tubular configurations noted 'MK4' and 'tub' in the legend. The symbols represent measured data from the indicated ion sources. The work functions and temperatures are displayed in the legend. The value of g_i/g_0 is approximated at 0.5 for these simulations. The poorly known electron affinity of Astatine is taken at 2.31 eV ([39] and Rothe, private communication). For a tubular configuration, $N = 20$ based on previous studies with positive tubular surface ion sources [40].

3.4 eV. Iodine and astatine are shown to be the most sensitive and challenging elements to ionize owing to their low electron affinities with respect to the ionizer materials used. It is noted that these calculations are for ionization efficiency only, independent of other properties such as diffusion from the target matrix, chemical reactivity, sticking times to interfaces, and molecule formation.

2.2. Sputter generation of negative ions

In sputter-type negative ion sources, negative ions are also formed on a low work function solid surface. However, the ion formation process is most commonly accepted as a two-step process that involves first the ejection of atomic and/or molecular particles from the surface via knock-on sputtering and then electron transfer between the surface and the ejected particles. The ionization of the sputtered particles is complicated by the dependence on the characteristic properties of the outgoing particles, the emitting surface, and the projectile ions as well as the mechanism of the ejection process. Various models have been proposed [41] for a theoretical description of the ionization process, including an electron tunneling model, a bond-breaking model, and a substrate-excitation model. However, there is still no theoretical model that can predict the secondary ion probability with sufficient accuracy for practical applications. An exponential relationship scaling of the ionization probability P^- of sputtered negative ions with the work function of the surface is predicted by the theoretical treatments and observed experimentally [42]

$$P^- \propto \exp\left(-\frac{\phi - E_a}{\varepsilon_0}\right), \tag{4}$$

where ε_0 is a characteristic parameter of the ion emission process and is reported to depend on the normal component of the ion emission velocity [43, 44]. Similar to negative surface ionization, P^- can be greatly enhanced by lowering the work function of the sputter site, which can be achieved with the addition of a sub-monolayer of alkali atoms such as cesium to the surface [45].

Cs-sputter negative ion sources are more versatile than negative surface ionization sources, but are unsuitable for ISOL generation of short-lived radioactive beams. The sputter target is also the production target for the radioactive species, so the area to be sputtered should match with the area irradiated by the production ion beam. Consequently, the primary production beam must overlap with the Cs-sputter ions and in turn with the resulting negative radioactive beam. This would adversely affect negative ion generation and extraction. On the other hand, Cs-sputter sources can be used for batch-mode generation of relatively long-lived RIBs where production and ionization are performed independently (see section 4.3). In fact, the batch-mode technique is one of the early approaches for producing negative ion beams of isotopes with lifetimes longer than a few hours [46–51]. A multi-sample Cs-sputter ion source was developed at HRIBF for batch-mode generation of RIBs of long-lived isotopes [52, 53]. Chemically active radioactive species are often released from target materials in a variety of molecular forms, for example, fluorine isotopes were found to be released from Al_2O_3 production targets primarily as AlF. Since the species of interest may be distributed in several mass channels in the form of these molecular sidebands, beam intensities of the desired radioactive species are diluted. The sputter method
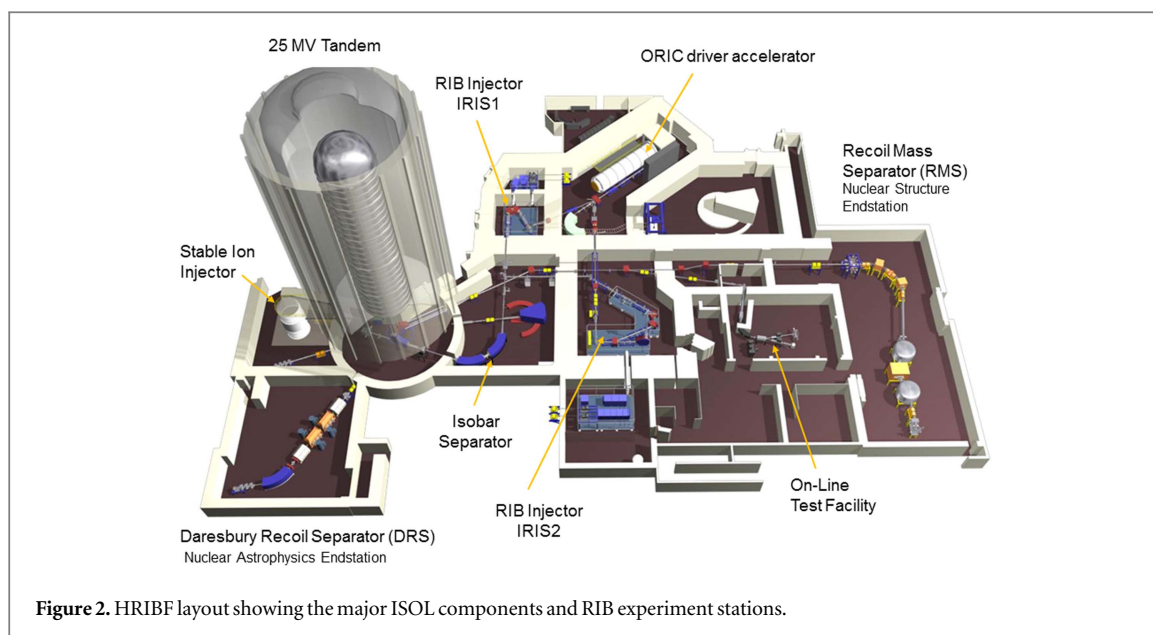
Figure 2. HRIBF layout showing the major ISOL components and RIB experiment stations.
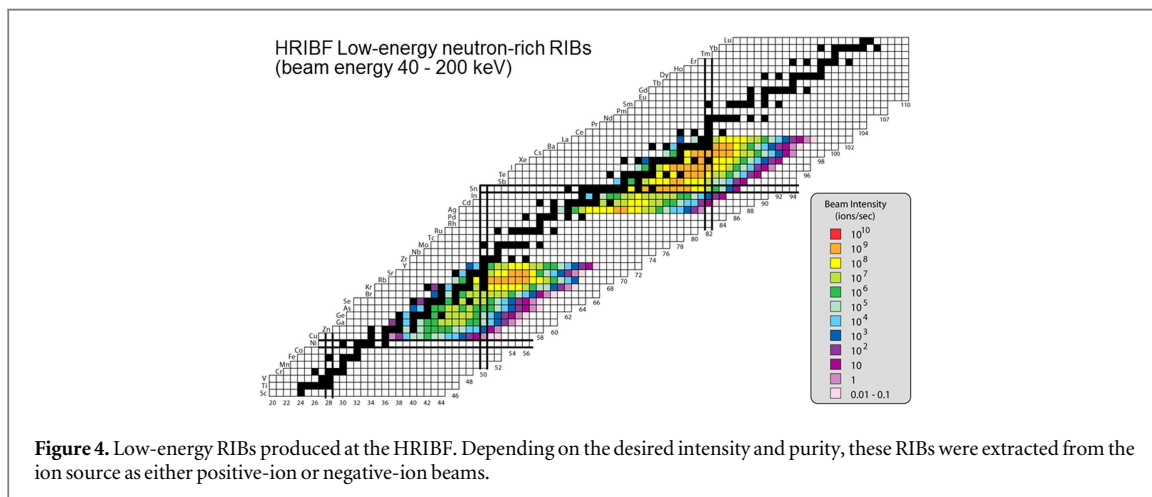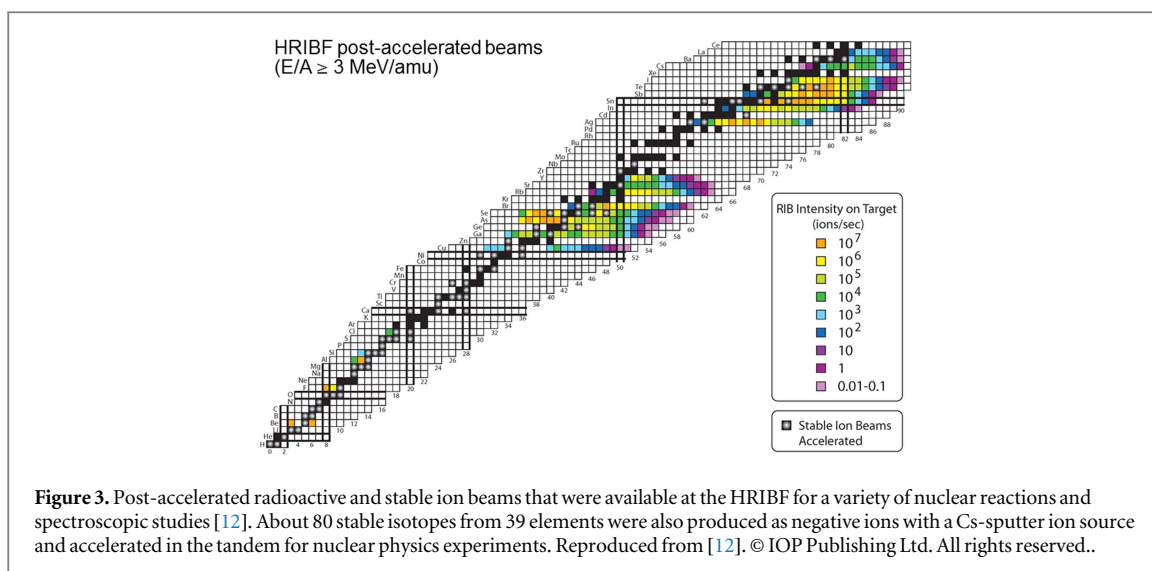
for negative ion formation is found to be an effective means for simultaneously dissociating molecular carriers and efficiently ionizing highly electronegative atomic constituents present in the molecule. A unique Cs-sputter negative-ion source was conceived [54, 55] at HRIBF that could solve the molecular sideband problem for ^{17,18}F beams. Details of these sputter-type ion sources are reported in section 4.

3. Production of negative RIBs at HRIBF

The HRIBF [12] at ORNL was a Department of Energy User Facility with a mission to deliver high-quality RIBs using the ISOL technique. The ISOL technique was implemented at HRIBF (figure 2) with the following major components: the Oak Ridge Isochronous Cyclotron (ORIC) driver accelerator, two RIB production systems—Injectors for Radioactive Ion Species (IRIS1 and IRIS2), and the 25 MV tandem electrostatic accelerator for RIB post-acceleration. The ORIC provided a light-ion beam (proton, deuteron, or alpha) which was directed onto a thick target mounted in a target-ion source (TIS) assembly located on IRIS1 or IRIS2. Radioactive atoms or molecules that diffused from the target material were transported to the ion source where they were ionized, extracted, and formed into a beam. Typically, the RIB (either positive or negative ions) was accelerated from the ion source at an energy of 40 keV and passed through the first-stage mass analyzer which selected beams of a single mass with resolving power of ~600:1 (FWHM). The mass-selected beam could then be sent through an optional Cs-vapor charge exchange cell before being further accelerated to 200 keV energy from the high voltage production platform and passed through the second-stage mass analyzer (isobar separator) with a mass resolving power ($M/\Delta M$) up to 100 00/1 depending on the emittance of the incoming beam. Next, the beam of negatively charged ions was injected into the 25 MV tandem for post acceleration. Alternatively, beams of either charge could be transported to the low-energy RIB spectroscopy station [56] where the decay properties of the isotopes were studied.

Negative ions at 200 keV were injected into the tandem electrostatic accelerator, which has a folded-geometry and has been operated with beam at terminal potentials up to 25.5 MV (highest in the world), and as low as 1 MV with excellent reliability. At the terminal, electrons were stripped away from the beam particles using thin carbon foils or a dilute gas. The resulting positive ions were selected based on energy, mass, and charge state by a 180° dipole magnet and subsequently accelerated down the high-energy side of the tandem. For light nuclei ($A < 80$), single-stripping allowed for acceleration up to at least 5 MeV per nucleon. For heavy ions ($A > 80$), a second foil stripper could be inserted at about a third of the way down the high energy column to strip to higher charge states to achieve higher energies. This capability enabled HRIBF to be the first RIB facility to accelerate $A = 130$ neutron-rich fission fragments above the Coulomb barrier. A 90° energy-analyzing dipole magnet mounted on a rotating platform at the base of the tandem high-energy tube selected the beam of interest and directed it into one of several beam lines for nuclear physics experiments.

Based on the capabilities of the driver cyclotron, ORIC, several types of RIB production targets were developed for the HRIBF [57]. ORIC provided proton beams up to 54 MeV, deuteron beams up to 49 MeV, and ^{4}He beams up to 85 MeV with intensities up to 20 μA for proton, 15 μA for deuteron, and 5 μA for ^{4}He on target. For neutron-rich RIBs, a uranium carbide target was developed to produce fission fragments via proton-

Figure 3. Post-accelerated radioactive and stable ion beams that were available at the HRIBF for a variety of nuclear reactions and spectroscopic studies [12]. About 80 stable isotopes from 39 elements were also produced as negative ions with a Cs-sputter ion source and accelerated in the tandem for nuclear physics experiments. Reproduced from [12]. © IOP Publishing Ltd. All rights reserved..

Figure 4. Low-energy RIBs produced at the HRIBF. Depending on the desired intensity and purity, these RIBs were extracted from the ion source as either positive-ion or negative-ion beams.

induced fission. While several uranium carbide target geometries and formats were developed, this was essentially a single target for many radioactive beams. On the other hand, radioactive beams on the proton-rich side of the nuclide chart required the development of several targets. Due to the low energy of the driver beam, the radioactive nuclei were produced with *A* and *Z* very close to the target nucleus, so unique production targets were developed for each element, including hafnium oxide targets for fluorine beams, silicon carbide targets for aluminum beams, and liquid germanium targets for arsenic beams. In all cases, the production targets and the ion sources developed at the HRIBF were designed such that any production target could be used with any ion source, so the best combination for a particular experiment could be used. Negative-ion sources were used extensively with oxide targets for fluorine beams and with uranium carbide targets to provide pure beams of bromine and iodine isotopes from fission.

The ISOL production technique was used at HRIBF to produce beams of more than 200 radioactive isotopes, including more than 175 neutron-rich species from fission of uranium (see figure 3). Many of these were post-accelerated to energies required for nuclear physics experiments (several MeV per nucleon) while others were used at low energies (40–200 keV) for decay studies (figure 4). More than 50 of those RIBs, including doubly magic ^{132}Sn, were available at intensities of 10^6 ions per second or greater. A careful comparison of figures 3 and 4 show a number of isotopes that are available as low-energy beams but are not available as post-accelerated beams. This is due to the fact that it is not possible to make a negative ion for some elements, including noble gases and specific elements such as Zn and Cd. The large gap in available beams from Zr to Pd is a general short-coming of the ISOL technique—these elements have very low vapor pressures even at high temperatures and thus will not diffuse out of the production target.

Most of the negative-ion beams at HRIBF were produced using a standard charge-exchange method in which radioactive species were first ionized as positive ions and then passed through a cell filled with Cs vapor to form a negatively charged ion beam. The most commonly used positive-ion source was the electron beam
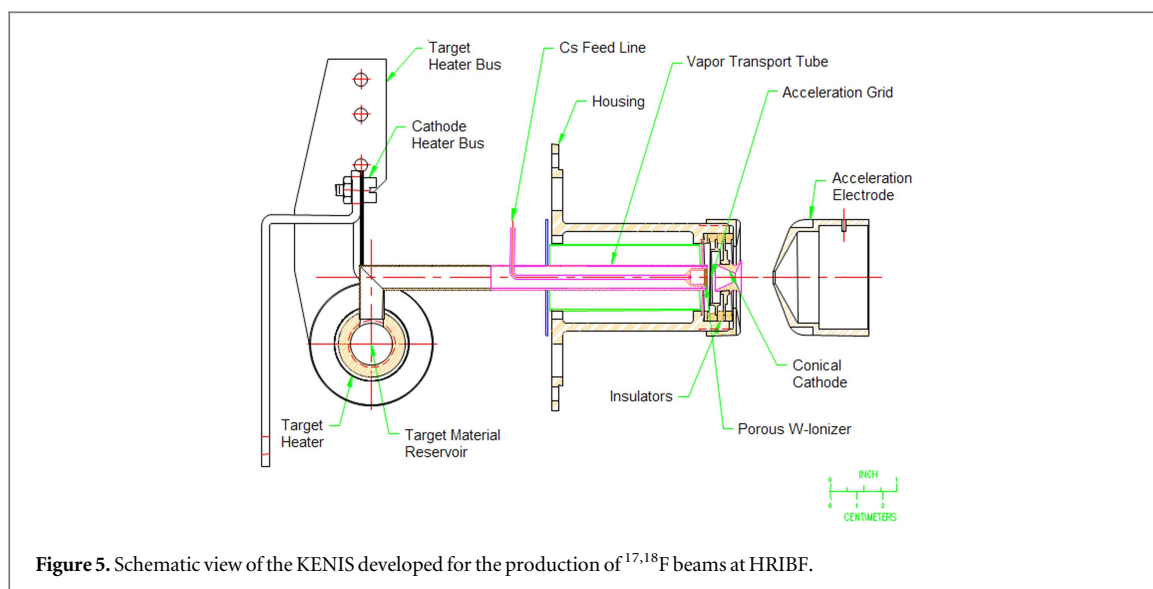
Figure 5. Schematic view of the KENIS developed for the production of ^{17,18}F beams at HRIBF.

plasma ion source (EBPIS) [58, 59]—a universal and efficient ion source that can ionize essentially any atomic or molecular species transported into the plasma volume. Nevertheless, negative-ion sources were needed to provide higher beam intensities and better beam purity for some radioisotopes. For example, the EBPIS is not selective and often generated beams with strong isobar contaminants that could not be readily separated by the magnetic isobar separator. In addition, the charge-exchange processes often resulted in rather large energy spreads in the negative-ion beams which in turn limited the isobar suppression capability of the electromagnetic isobar separator. In these cases, additional isobar suppression methods or steps were necessary. Considerable effort was put forth to investigate potential negative-ion sources based on different ionization methods, including surface ionization [37, 60, 61], plasma-sputtering [62], Cs-sputtering [54, 63], and electron-beam plasma [64]. Three negative-ion sources that have been successfully used online for RIB production are described in the next section.

4. Negative-ion sources for the production of RIBs

4.1. Kinetic-ejection negative-ion sources (KENIS)

The kinetic-ejection negative-ion source (KENIS) [54] was first developed at HRIBF for the production of ^{17}F and ^{18}F beams. Radioactive ^{17,18}F beams are of considerable interest for studying nuclear astrophysical reactions responsible for element synthesis in the Universe. They were produced at HRIBF through the respective reactions ^{16}O(d, n)^{17}F or ^{18}O(α, pn)^{18}F using thin fibrous oxide materials such as A1$_2$O$_3$, Y$_2$O$_3$, ZrO$_2$, or HfO$_2$ [57]. Although negative surface ionization sources with LaB$_6$ ionizers have been shown to be highly efficient for halogens such as Cl, Br, and I, their efficiencies for negative F ions are extremely poor [22, 55]. This could be explained by the observation [55, 65] that fluorine isotopes were released to the ion source primarily in molecular forms, such as AlF, which have relatively low electron affinities and thus small probabilities for negative surface ionization. The charge-exchange method with the EBPIS has been used for generating negative F beams, but ionization efficiencies for the fluorine compounds were found to be on the order of 1% and the desired F ions were distributed in several molecular sidebands. Moreover, the charge-exchange efficiencies from the positive molecular ions to negative atomic fluorine ions, e.g., AlF$^+$ → F$^-$, were also very low. Therefore, an efficient negative-ion source was needed to dissociate the molecules and ionize the atomic F simultaneously. This requirement has led to the development of KENIS, which is a unique Cs-sputter negative-ion source for direct production of negative ^{17,18}F beams.

A schematic view of the HRIBF KENIS is shown in figure 5. The ion source and the target assembly are designed with the following principal components. A Ta target-material reservoir is attached to a Ta vapor-transport tube. A 50% porosity W-ionizer for formation of intense Cs$^+$ beams via surface ionization, is co-axially located in the center of and fixed to the exit end of the vapor-transport tube. Cs vapor is transported to the porous W-ionizer from an externally located Cs-oven through an independent tube, co-axially located within the vapor-transport tube and weld attached to the W-ionizer. A negatively biased acceleration grid accelerates the Cs$^+$ beams to energies of 150–300 eV to bombard the inner surface of a negatively biased, conical geometry Ta cathode. Annular apertures, located between the vapor-transport tube and the W-ionizer allow the radioactive species emerging from the target reservoir to flow through the acceleration grid and deposit on the
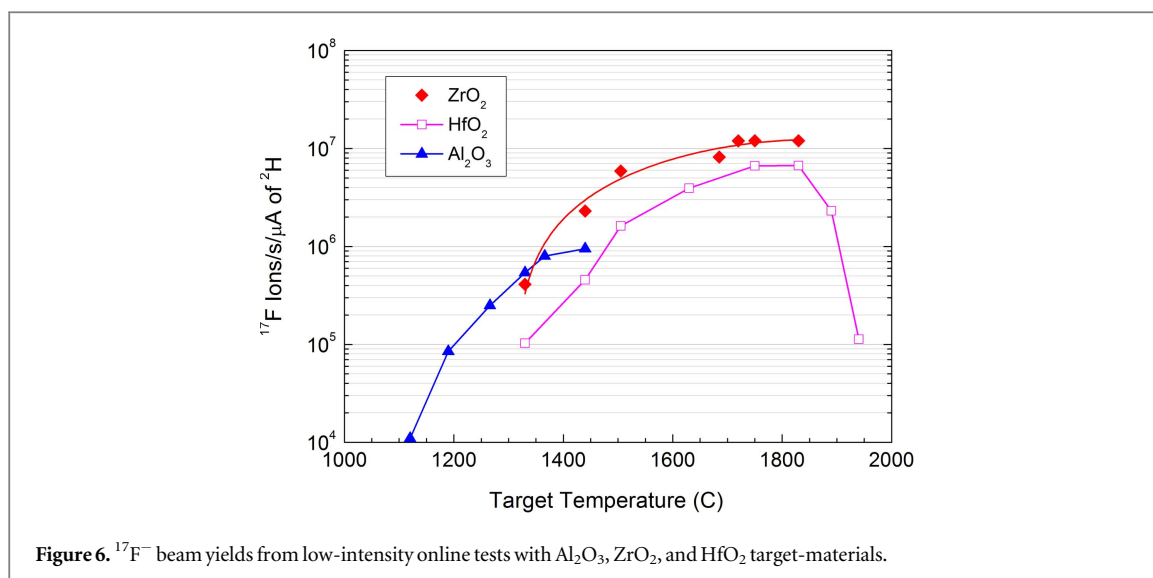
Figure 6. $^{17}F^-$ beam yields from low-intensity online tests with Al_2O_3, ZrO_2, and HfO_2 target-materials.

conical cathode surface where they are sputtered by positive Cs ions and a fraction of them are re-emitted as negative ions. The Cs^+ beam not only serves to eject particles from the cathode surface, but also lowers the work function of the surface, thereby greatly enhancing the yield of negative ions. Negative-ion beams are extracted through a circular aperture (diameter $\phi = 2$ mm) in the apex of the cathode cone.

In offline studies, the performance of this source was evaluated by injecting SF_6 molecules into the high-temperature target reservoir filled with fibrous Al_2O_3 materials. SF_6 decomposes and reacts with Al_2O_3 at the target operating temperatures to form aluminum fluoride molecules, which can be effusively transported to the ion source. The mass spectrum of the negative ions extracted from the KENIS was clean and simple, with essentially 100% of the F-ions appearing in the mass 19 channel. As a reference, the positive ions generated using the EBPIS contained various fluoride molecular ions, with only about 13% of the total fluorine in the atomic F^+ channel [54]. To measure the ionization efficiency of the KENIS, SF_6 was introduced into the source through a calibrated leak at a precisely controlled rate. The ratio of the F^- ions detected to the number of neutral fluorine atoms injected was the overall ionization efficiency and was measured to be 5%–7%.

In low intensity, online tests, mass-analyzed beams of $^{17}F^-$, up to 10^7 ions s^{-1} μA^{-1} of deuteron beam (figure 6) were obtained using fibrous ZrO_2 and HfO_2 target-materials through the $^{16}O(d, n)^{17}F$ reaction. In general, ion yields increased with increasing target temperature until the target material started to dissociate. At $\sim 1800\,°C$, ZrO_2 and HfO_2 started to dissociate and the high vapor pressure of oxygen and oxide molecules reduced the efficiency of the ion source. This effect occurred at much lower temperatures for Al_2O_3 (around $1400\,°C$) when the alumina was in contact with tantalum or other refractory metals. During online operations, with the KENIS installed on the IRIS1 RIB production platform, $^{17,18}F$ isotopes were produced using HfO_2 cloth targets. This HfO_2 cloth consisted of thin fibers of about 5 μm diameter woven together to form a low-density, rugged material that was free from volatile impurities. However, the fastest and most efficient transport mechanism from the target to the ion source was the AlF molecule, so a layer of Al_2O_3 foam was wrapped around the HfO_2 target to provide the required Al atoms. The AlF molecule was transported to the ion source where it was collected on the cone and negative fluorine ions were subsequently sputtered off the cone by the Cs^+ ions generated in the W ionizer and accelerated to about 300 eV by the negative potential on the cone.

The KENIS was the primary ion source for generation of negative $^{17,18}F$ beams at the HRIBF from 1998–2012, with post-accelerated ^{17}F beam intensities reaching 10^7 particles/second and ^{18}F beam intensities on the order of 2×10^5 particles/second. The ^{18}F beam was mixed with the stable isobar ^{18}O at a ratio of $^{18}O/^{18}F \sim 8$. Pure ^{18}F beam could be obtained by fully stripping the beam to 9^+ charge state, with some loss in intensity. The average TIS lifetime during online operation was about 1200 h (3000 μAh) with the main failure mode being low fluorine yields due to beam-induced target damage. Availability of these fluorine beams enabled many experiments, including direct measurements of astrophysically important proton capture cross sections, e.g. the $^{18}F(p, \alpha)^{15}O$ and $^{17}F(p, \gamma)^{18}Ne$ reaction cross sections [66], and measurements of elastic scattering and breakup of ^{17}F on a ^{208}Pb target and simultaneous two-proton emission from an excited state in ^{18}Ne [67].

4.2. Negative surface ionization sources
Negative surface ionization sources are generally characterized by a high degree of ion beam purity (chemical selectivity) and high efficiencies for highly electronegative species. These advantages have been utilized for negative RIB generation of high-EA elements such as the Group VIIA halogens (Cl, Br, I and At).
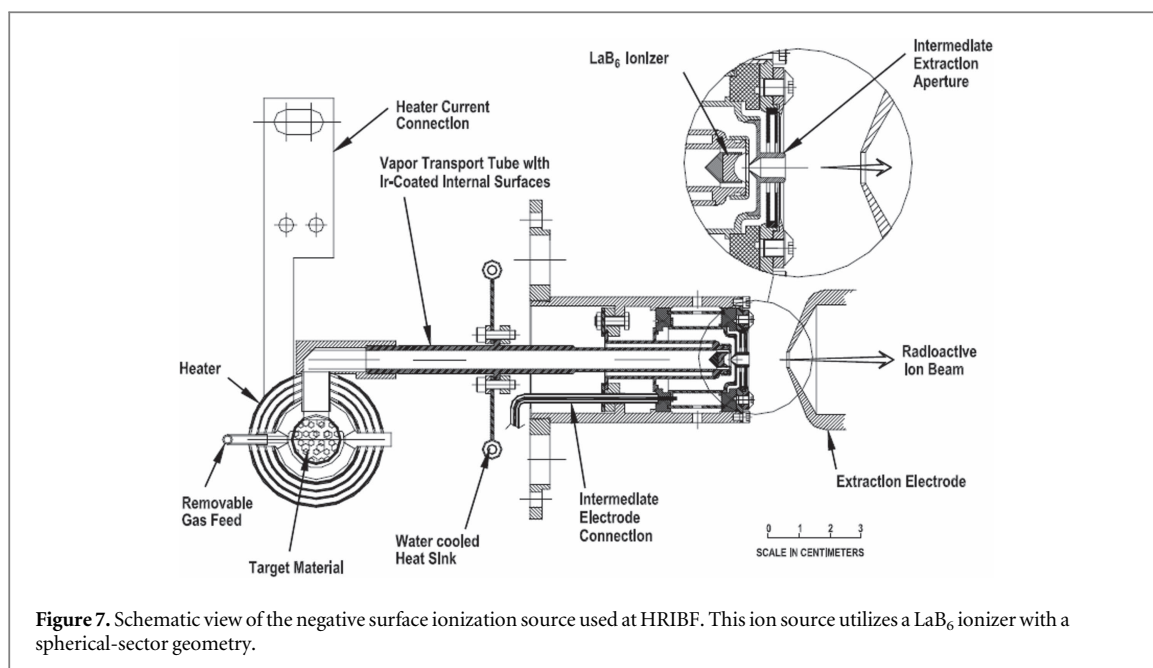
Figure 7. Schematic view of the negative surface ionization source used at HRIBF. This ion source utilizes a LaB$_6$ ionizer with a spherical-sector geometry.
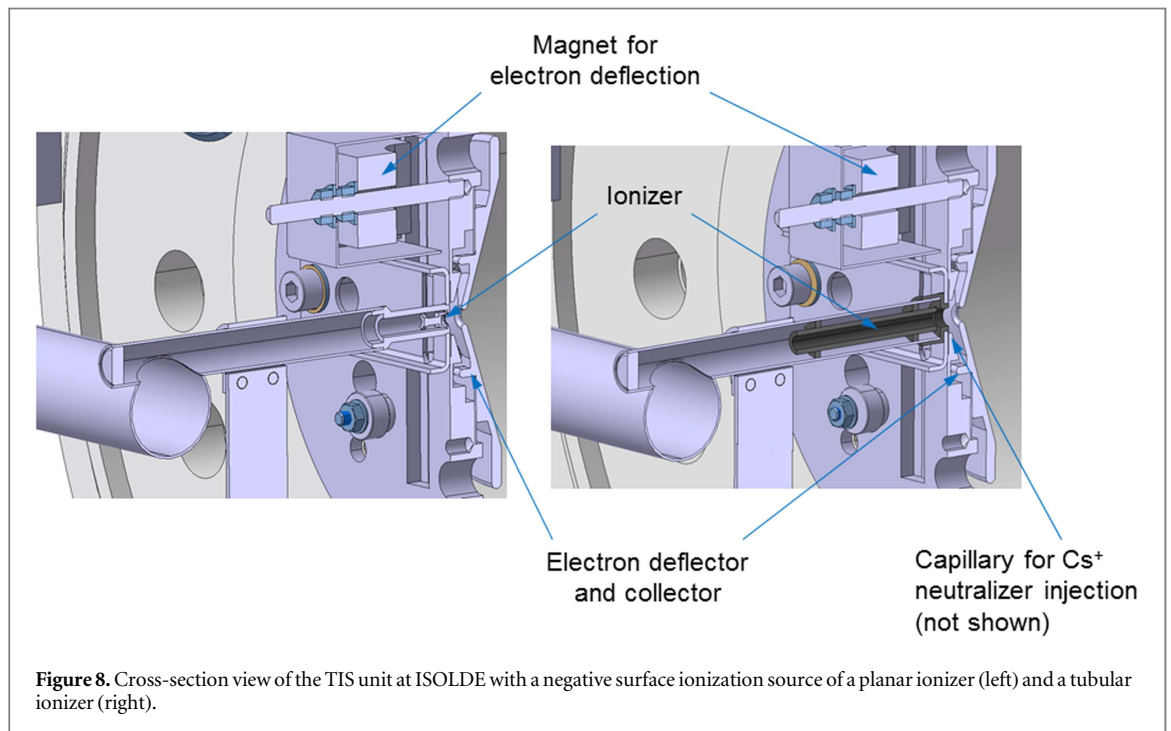
4.2.1. Negative surface ionization source at HRIBF

At the HRIBF, positive RIBs of the group VIIA elements, e.g., bromine and iodine, were available with the EBPIS and uranium carbide targets, but they were strongly mixed with isobars of the neighboring elements. For example, the mass-88 positive ion beam consists of 7% Br, 33% Kr, and 60% Rb. Even after the Cs-vapor CEC, this negative-ion beam was still a mixture of 26% Br and 74% Rb. A negative surface ionization source with a spherical-sector LaB$_6$ ionizer [60, 61] was developed to address this problem. A schematic view of the ion source and target assembly is given in figure 7.

Similar to the KENIS, the ion source is connected to the target reservoir via a Ta vapor-transport tube (8.5 mm inner diameter) and the spherical-sector LaB$_6$ ionizer is co-axially located at the exit end of the transport tube. The ionizer (spherical radius: 2.5 mm; diameter: 4.3 mm) is machined from a solid LaB$_6$ rod and pressed into a 6 mm diameter Ta holder. Atomic or molecular species released from the target reservoir enter the ionization region through the annular slots surrounding the ionizer holder. The spherical-geometry, extraction optics are designed to focus negative-ion beams through a very small extraction aperture (0.41 mm diameter) through which all charged and neutral particles must pass before leaving the ionization volume of the source. The neutral species will strike the hot extraction electrode bounce back and forth between the hot surfaces of the ionization volume, eventually striking the hot LaB$_6$ surface. Thus, this geometry enhances the probability for ionization of highly electronegative species that enter the volume. The negatively ionized particles are then accelerated and focused through the small aperture by the electric field produced between the spherical geometry ionizer and the extraction electrode that is maintained at positive potential. This ion source also generates large currents of electrons, which are deflected away from the extraction electrode to a grounded plate by a magnetic field perpendicular to the beam axis, which is produced by an electromagnet mounted outside the vacuum chamber along with internal pole pieces near the extraction aperture. In offline studies, the transport tube was heated resistively to 1400 °C–2000 °C by passing an electric current through the tubular structure, while the temperature of the LaB$_6$ ionizer was typically operated around 1650 °C, below the onset (1730 °C) for thermal dissociation of LaB$_6$, as calculated using the software HSC Chemistry [68]. The performance of the ion source for generating negative beams of Cl and Br was investigated by feeding AlCl$_3$ and AlBr$_3$ vapors at low-feed rates into the source and ionization efficiencies up to about 28% and 15% for Cl$^-$ and Br$^-$, respectively, were obtained [61, 69].

In online operations, the LaB$_6$ source has shown to be able to provide isobarically pure beams of Br and I isotopes. Table 2 lists the production rate of Br and I isotopes from proton-induced fission of ^{238}U in a uranium carbide target irradiated with a 54 MeV proton beam. Also, listed are the measured negative ion rates, the total TIS efficiency, and the negative-ion beam intensities injected into the post-accelerator when a 5 μA proton driver beam was used. As noted, an overall TIS efficiency of 7% was obtained for the relatively long-lived ^{83}Br, in close agreement with the offline ionization efficiency of 15% for Br. Despite the somewhat low ionization efficiencies for Br and I isotopes, the negative-ion yields for Br isotopes were about 25 times greater than the positive-ion yields from the EBPIS followed by charge exchange and the beam was pure, no contamination with

Table 2. Measured ion yields from a UC target coupled to the LaB$_6$ surface ionization source at HRIBF.

Isotope	Half-life	In-target production rate ions s^{-1} μA^{-1} ^{1}H$^+$	Negative-ion TIS yield ions s^{-1} μA^{-1} ^{1}H$^+$	TIS efficiency (%)	Beam injected into the tandem with 5 μA, 54 MeV ^{1}H$^+$
^{83}Br	2.40 h	9.04E+07	6.4E+06	7.1	3.2E+07
^{84g}Br	31.8 m	1.12E+08	5.2E+06	4.6	2.6E+07
^{85}Br	2.90 m	1.34E+08	3.2E+06	2.4	1.6E+07
^{86}Br	55.1 s	1.32E+08	8.5E+05	0.6	4.3E+06
^{87}Br	55.6 s	1.11E+08	1.5E+06	1.3	7.5E+06
^{88}Br	16.3 s	6.82E+07	2.3E+05	0.3	1.2E+06
^{132m}I	1.39 h	1.35E+08	8.2E+0	0.61	4.1E+06
^{132g}I	2.3 h	1.35E+08	7.3E+05	0.54	3.7E+06
^{134m}I	3.5 m	3.60E+08	1.5E+06	0.42	7.5E+06
^{134g}I	52.5 m	4.13E+08	2.7E+06	0.65	1.4E+07
^{136m}I	46.9 s	2.20E+08	1.9E+06	0.87	9.5E+06
^{136g}I	83.4 s	2.26E+08	1.2E+06	0.53	6.0E+06
^{137}I	24.5 s	2.25E+08	2.2E+05	0.10	1.1E+06
^{138}I	6.2 s	7.65E+07	2.3E+04	0.03	1.2E+05

Figure 8. Cross-section view of the TIS unit at ISOLDE with a negative surface ionization source of a planar ionizer (left) and a tubular ionizer (right).

isobars from neighboring elements. For iodine isotopes, the gain in yield from the LaB$_6$ ion source was about a factor of 10 greater than achieved from the EBPIS followed by charge exchange and again, the beam was pure.

4.2.2. Negative surface ionization sources at ISOLDE

Negative surface ionization sources with planar and hollow-tube ionizers have been developed at ISOLDE. As discussed in section 2.1, the overall ionization efficiency can be significantly enhanced with the tubular geometry as given by equation (3). Figure 8 shows the cross-section view of the TIS assemblies with a planar-ionizer source (MK4) and a tubular-ionizer source. The important functional elements for the ion source operation are indicated, namely a magnet to create a perpendicular field of about 0.08 T to deflect the emitted electrons, an electrostatic deflector/collector typically polarized at 1 kV (0–3 kV range), made of copper, to collect the electrons. For the planar MK4 ion source, the LaB$_6$ sintered pellet is held in place with a molybdenum fitting in the tantalum cavity, while for the tubular ion source, two Molybdenum rings are used to hold the tubular ionizer in the tantalum transfer line. A capillary is used to inject Cs vapor to provide positive charge compensation of the emitted electrons with counter-propagating Cs$^+$ ions, aiming at creating a positive plasma well in the tube to

Table 3. Measured ion yields from UC target using the MK4 LaB$_6$ surface ionization source at ISOLDE.

Isotope	Half-life	Yield/Production rate (ions s^{-1} μA^{-1} ^{1}H$^+$)	TIS efficiency (%)
^{38}Cl	37.2 m	1.6 10^5	
^{39}Cl	56 m	1.1 10^5	
^{40}Cl	81 s	4.3 10^4	
^{41}Cl	38.4 s	1.4 10^4	
^{42}Cl	6.9 s	1.1 10^3	
^{43}Cl	3.3 s	3.0 10^2	
^{82}Br	6.13 m	7.3 10^6	0.55
^{83}Br	2.37 h	1.8 10^6	8.4
^{85}Br	2.90 m	9.6 10^5	
^{87}Br	55.6 s	2.1 10^5	1.0
^{88}Br	16.3 s	2.7 10^5	1.5
^{89}Br	4.4 s	8.4 10^4	
^{90}Br	1.9 s	1.5 10^3	0.13
^{91}Br	0.54 s	2.5 10^3	
^{92}Br	0.34 s	1.4 10^3	0.056
^{122}I	3.6 m	4.4 10^4	
^{137}I	24.2 s	1.3 10^5	
^{138}I	6.4 s	7.3 10^5	
^{139}I	2.3 s	1.7 10^4	
^{140}I	0.86 s	3.3 10^3	
^{141}I	0.43 s	3.5 10^3	

trap the negative ions. The tubular negative-ion source has been developed with different low work function materials including a GdB$_6$ ceramic tube, a BaO/SrO impregnated W tube, and Ir$_5$Ce metallic alloys. Ionization efficiencies for Br$^-$ and I$^-$ of 10% have been measured when operating the ion source at 1700 °C.

The MK4 ISOLDE negative-ion source equipped with a planar ionizer is the traditional ISOLDE negative-ion source that was developed in the eighties by Vosicki and collaborators and used with a number of different target materials to produce halogen beams—with the exception of fluorine beams. At that time, the radioisotopes were produced with a CW 600 MeV proton beam from the synchro-cyclotron impinging target materials such as niobium and mixed niobium thorium powders, tantalum and mixed tantalum thorium foils, and uranium carbide [22]. This type of ion source was again used to produce RIBs after the ISOLDE facility was moved to the proton synchrotron booster to use its pulsed 1.4 GeV proton beam [4] to produce radioactive nuclei. In table 3, we present the beam intensities for isotopes of Cl, Br, and I from the TIS unit UC263A-MK4 operated online in 2005, which combined the MK4 with a uranium carbide target. The unit was operated at target temperatures of 1800 °C and 2000 °C while the LaB$_6$ pellet was at 1300 °C.

As seen in table 3, the reported TIS efficiency, which takes into account the efficiencies for all of the processes going from in-target production to ion beam extraction, decreases with the half-lives of the isotopes of a given chemical element. This trend was further analyzed by measuring the temporal isotope release function of the TIS unit, collecting and analyzing the so-called release curves [70], exploiting the pulsed nature of the proton beam of the PSB and time-dependent isotope activities collected with a tape station [71]. The release function $p(t)$ takes the form:

$$p(t) = A\left(1 - \exp\left(\frac{-t\ln(2)}{t_r}\right)\right)\left(\alpha\exp\left(\frac{-t\ln(2)}{t_f}\right) + (1-\alpha)\exp\left(\frac{-t\ln(2)}{t_s}\right)\right). \tag{5}$$

The extracted parameters from the fits to the measured release profiles for Cl, Br, and I from a LaB$_6$ ion source are reported in table 4. Figure 9 shows that the ionized fractions for the bromine isotope series as a function of their half-lives (solid line), computed from the release curve for Br and the ion source efficiency, compare well with the released ionized fractions computed using the in-target production and measured beam intensities of the Br isotopes (full diamonds). The ion source efficiency was initially 8.4%, measured with the long-lived ^{83}Br beam. It however rapidly dropped to 0.1%, which was attributed to the poisoning of the LaB$_6$ with the outgassing of the carbide target. The systematic comparison in figure 9 was done after the poisoning had taken place and no further decrease in source efficiency was observed. The results thus indicate that the drop in efficiencies for exotic isotopes is related to the release characteristics of the TIS unit, and not to the ionization process itself.

The LaB$_6$ MK4 ion source was operated again in 2016 with a mixed Th/Ta foil target, for fission fragment and spallation products, in particular Astatine beams. The reported ion yields are ^{38}Cl: 1.10^5/μC, ^{85}Br: 1.10^4/μC, ^{128}I: 9.10^5/μC, and ^{204}At: 9.10^3/μC, respectively. The unit was operated at target temperature of

Table 4. Release time characteristics for the unit UC264A-LaB$_6$.

Isotope	t_r(ms)	α	t_f(ms)	t_s(ms)
Cl	85 000	0.25	79	7180
Br	305	0.87	3865	116 000
I	83	0.65	587	9550
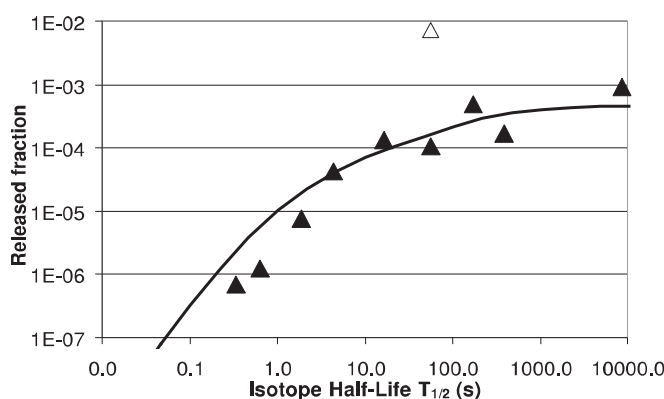
Figure 9. TIS efficiency expressed as released fraction for Br radioisotopes from the UC264A target unit. — calculated with the release curve and the ion source efficiency for ^{83}Br, ▲calculated from in-target production rates and measured ion intensities (Δ calculated before poisoning of the LaB$_6$ ionizer).

1900 °C and ion source temperature of 1200 °C and displayed slower release characteristics when compared to the UC$_x$ target coupled with positive ion sources at 2000 °C. Although halogens are volatile elements, they are reactive elements and prone to strong adsorption and reactions with various structural materials. Data on surface adsorption and desorption properties have been documented for transition metal interfaces such as tantalum and molybdenum [72]. The absolute desorption rates are found in the $1–8 \times 10^{14}$ s^{-1} range and enthalpies in 3.7–5.1 eV ranges for F, Cl, and Br. This provides desorption times in the 0.5–4.0 ms range. When folding this with an estimated number of interactions with a foil target (100 000) or with the structural material (500), this provides an overall effusion delay time of the order of 0.25–400 s for TIS temperatures up to 1300 °C, well in the range to account for the slow release properties and reduced efficiencies for exotic isotopes as shown in figure 9 and table 4 [73].

The electron current measured on the collector plate can be used to assess the thermionic emission of the LaB$_6$ pellet, from which its effective work function can be assessed. The electron current saturated above 2 kV applied on the deflector plate. A similar value of 2 kV was also used by Pelletier *et al* [35] to determine the work function of LaB$_6$ sintered pellets. Figure 10 shows the dependence of emitted electron current I on LaB$_6$ ionizer temperature, expressed as $\log(I/T^2)$ versus e/kT (so-called Richardson plot [74]), for the TaThO576-MK4 unit operated in 2016 at ISOLDE, together with the electron emission currents measured with various MK4 units previously operated at ISOLDE-SC. It can be seen that the historical MK4 ion sources were operated with a LaB$_6$ whose work function was close to 2.9 eV, somewhat larger than the 2.66 eV found for a nominal LaB$_6$ material.

4.3. Batch-mode Cs-sputter negative-ion sources

Negative-ion beams of relatively long-lived radioactive isotopes can be generated using Cs-sputter ion sources in batch mode. In this mode, long-lived radioactive isotopes are either produced via direct irradiation of the sputter target and then transferred to a Cs-sputter source or the radioisotope may be produced in a thick target, chemically separated from the target matrix, mixed with metal powder, formed into a sputter target, and inserted into a Cs-sputter ion source. Either way, this technique avoids the high target temperatures required for fast diffusion and fast effusive-flow to the ion source. Two Cs-sputter ion sources have been designed and evaluated at HRIBF for this application: a batch-mode Cs-sputter source and a multi-sample Cs-sputter source [52, 53]. As illustrated in figure 11, both are based on the previously developed single-sample Cs-sputter sources [75] with a conical geometry, W-surface ionizer for surface ionization of Cs atoms and similar ion optics for accelerating Cs$^+$ ions and extracting negative ions. The batch-mode source allows for sequential (without opening the vacuum system) on-line production and ionization of moderately long-lived species. That is, the species of interest are produced by irradiating the target materials with light-ion beams from the ORIC for an optimum time based on the half-life and the target is then transferred to the ion source position to be sputtered
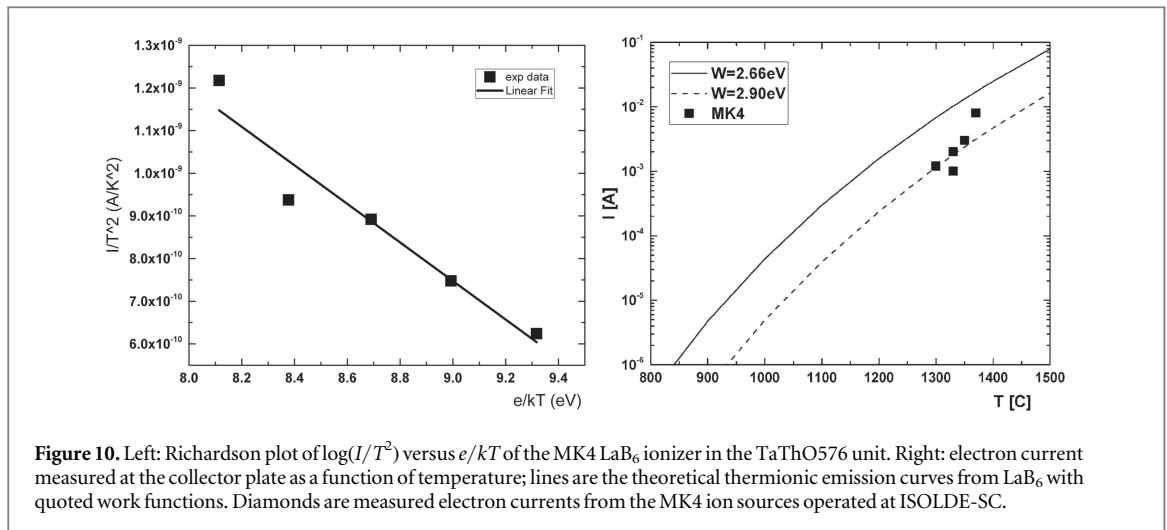
Figure 10. Left: Richardson plot of $\log(I/T^2)$ versus e/kT of the MK4 LaB$_6$ ionizer in the TaThO576 unit. Right: electron current measured at the collector plate as a function of temperature; lines are the theoretical thermionic emission curves from LaB$_6$ with quoted work functions. Diamonds are measured electron currents from the MK4 ion sources operated at ISOLDE-SC.
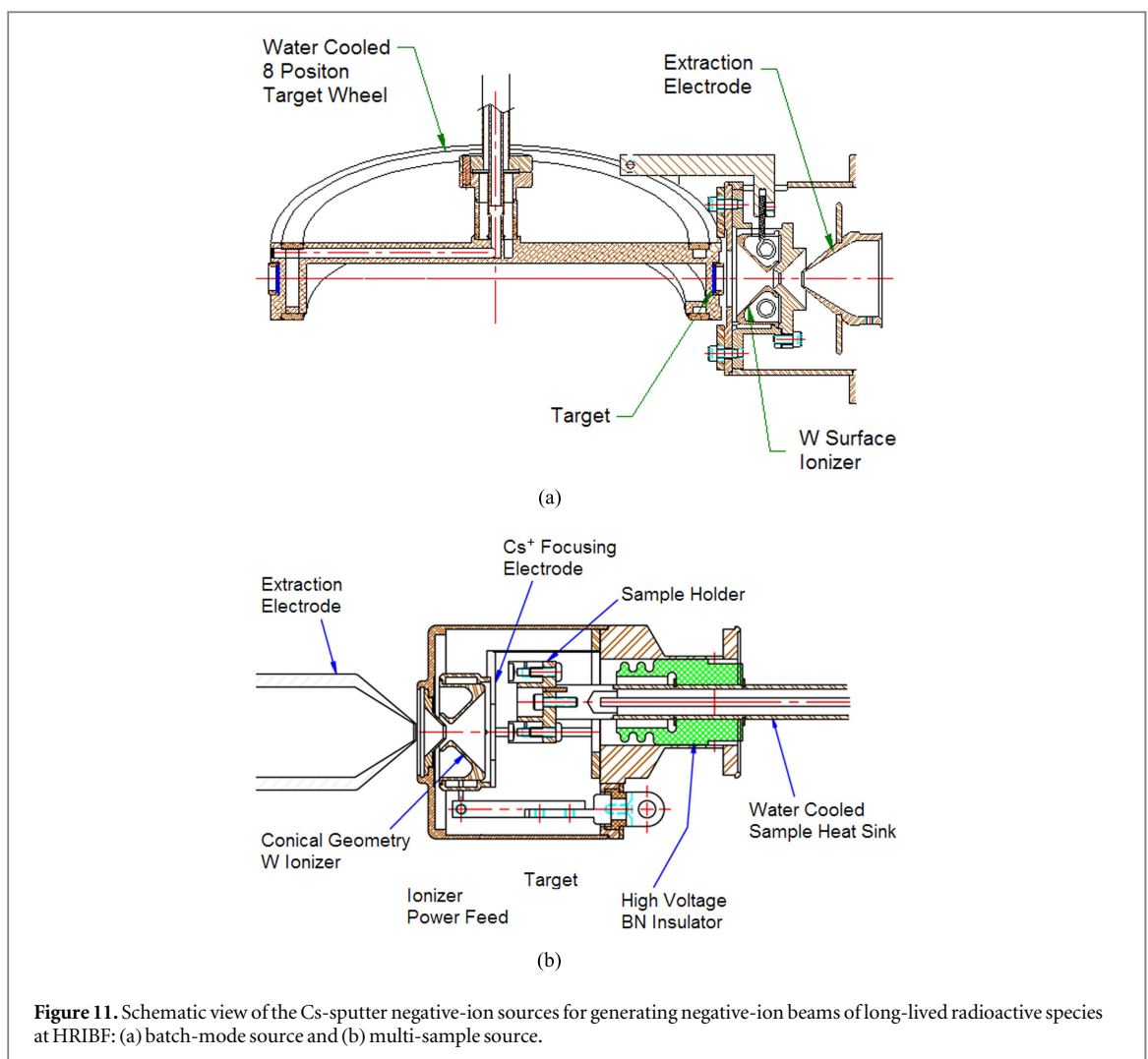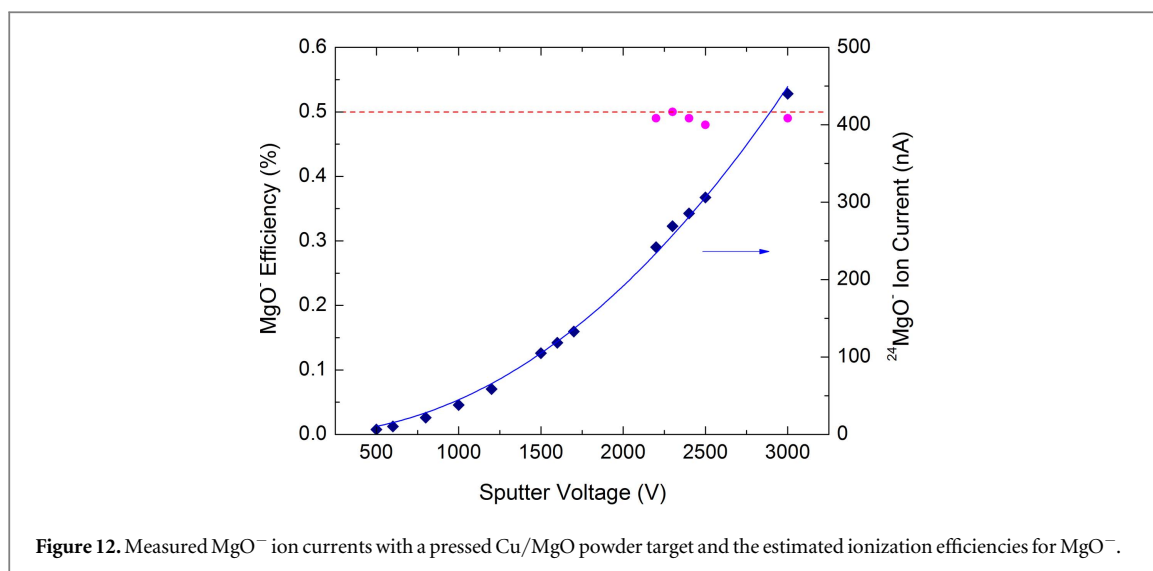

Figure 11. Schematic view of the Cs-sputter negative-ion sources for generating negative-ion beams of long-lived radioactive species at HRIBF: (a) batch-mode source and (b) multi-sample source.

with a 1–5 keV Cs$^+$ beam. A second target can be irradiated with ORIC beams while generating negative-ion beams from the initial target. This source was conceived and tested for the generation of ^{56}Ni$^-$ ($T_{1/2} = 6.077$ d) beams, but could be employed for the generation of several other species with lifetimes in excess of a few hours, such as ^{18}F ($T_{1/2} = 109.77$ min).

The multi-sample source was designed for batch-mode generation of long-lived species and was used to deliver beams of ^{7}Be ($T_{1/2} = 53.22$ d), ^{10}Be ($T_{1/2} = 1.51 \times 10^6$ yr), ^{26g}Al ($T_{1/2} = 7.17 \times 10^5$ yr), and ^{82}Sr ($T_{1/2} = 25.55$ d), which can be produced offline, processed chemically, and placed into the Cs-sputter ion source. It

Figure 12. Measured MgO$^-$ ion currents with a pressed Cu/MgO powder target and the estimated ionization efficiencies for MgO$^-$.

employs a small (30 mm diameter) sample wheel made of copper that can also hold up to eight, 6.4 mm diameter sputter samples and can be remotely indexed under vacuum to select the desired sample. This source was specifically designed for providing radioactive ^{7}Be$^-$ beams for the nuclear astrophysics experiment at HRIBF to directly measure the ^{7}Be(p, γ)^{8}B reaction cross section in inverse kinematics, ^{1}H(^{7}Be,^{8}B)γ, with a windowless hydrogen target and the Daresbury recoil separator [76]. The ^{7}Be(p, γ)^{8}B reaction is important for understanding the observed flux of solar neutrinos from the Sun. Since Be does not form stable atomic negative ions, molecular ions such as BeO$^-$ are commonly used for injection into tandem accelerators in which the oxygen atoms are removed by a stripper foil at the terminal. The sputter samples for ^{7}Be beams were pressed copper powder containing a small amount of ^{7}BeO. The production of the molecular negative ions was evaluated in offline tests [53] with MgO instead of BeO because MgO is chemically similar to BeO and posed no health hazards. Two types of pressed powder sputter targets were tested: Cu and Ag mixed with 3% MgO by weight. Similar or higher MgO$^-$ currents were obtained with the Cu targets. The ionization efficiency for MgO$^-$ was estimated based on the measured MgO$^-$ and Cs$^+$ ion currents and the sputter yields reported in literature. A typical efficiency obtained in such a way was near 0.5%, as shown in figure 12. It has been suggested [77, 78] that the ionization efficiency for BeO$^-$ could be a factor of 3–5 larger than that of MgO$^-$. Therefore, the estimated ionization efficiency for BeO$^-$ was about 2% with this multi-sample source.

The production of ^{7}Be beams was a collaboration between the University of North Carolina, the Colorado School of Mines, and the HRIBF. The radioactive ^{7}Be was produced at the Triangle Universities Nuclear Laboratory (TUNL). Samples of lithium metal were activated at TUNL using a 10 MeV beam of protons from the FN tandem accelerator, producing ^{7}Be via the ^{7}Li(p, n)^{7}Be reaction. Up to 50 mCi of ^{7}Be per day were produced using proton beam intensities of about 10 μA. The activated lithium slugs containing about 300 mCi of ^{7}Be were shipped to HRIBF, where a simple wet chemical process was performed to separate the ^{7}Be from the lithium. The separated ^{7}Be was added to a copper powder matrix, converted to an oxide (^{7}BeO), and pressed into a sputter sample designed for use with the multi-sample sputter source. The influence of the cathode geometry, chemical composition and ion source parameters on the production of ^{7}BeO$^-$ beam was studied in a series of tests at the online test facility at HRIBF. Figure 13 shows the ^{7}BeO$^-$ beam currents measured as a function of time from two independent samples, each containing 1 mCi of ^{7}Be (2.5 $\times$ 10^{14} atoms) within a copper metal matrix. Average beam intensities of about 1–2 million ^{7}BeO$^-$/second were obtained under good operating conditions, and a single sample produced useable beams for about a week with a total efficiency of about 0.5%–1.0% for production of ^{7}BeO$^-$ beam.

For the ^{1}H(^{7}Be, ^{8}B)γ measurement [76], a Cu/^{7}BeO sample with 120 mCi of ^{7}Be (3 $\times$ 10^{16} atoms) was used. The ^{7}BeO$^-$ beam from the multi-sample source was typically 20 pA, monitored with a movable tape collector and a HPGe detector system. During the 5 d experiment, the total ^{7}Be$^-$ output (measured at the tape system) was about 5.2 $\times$ 10^{13} ions, corresponding to 0.21% of the total sample activity. During this experiment, the post-accelerated beam intensity peaked at about 2 $\times$ 10^7 ^{7}Be/second on target. Similarly, beams of ^{10}Be$^-$, ^{26g}Al$^-$, and ^{82}Sr [79] were obtained with the multi-sample source and delivered to experiments with peak intensities more than 10^7 ions s^{-1}.
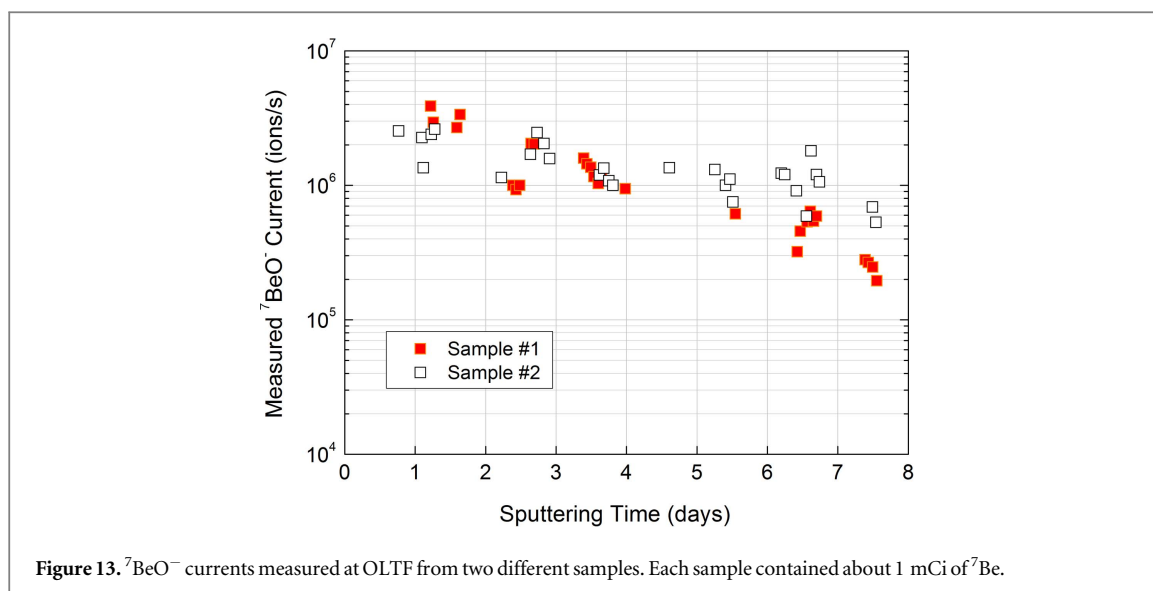
Figure 13. ^{7}BeO$^-$ currents measured at OLTF from two different samples. Each sample contained about 1 mCi of ^{7}Be.
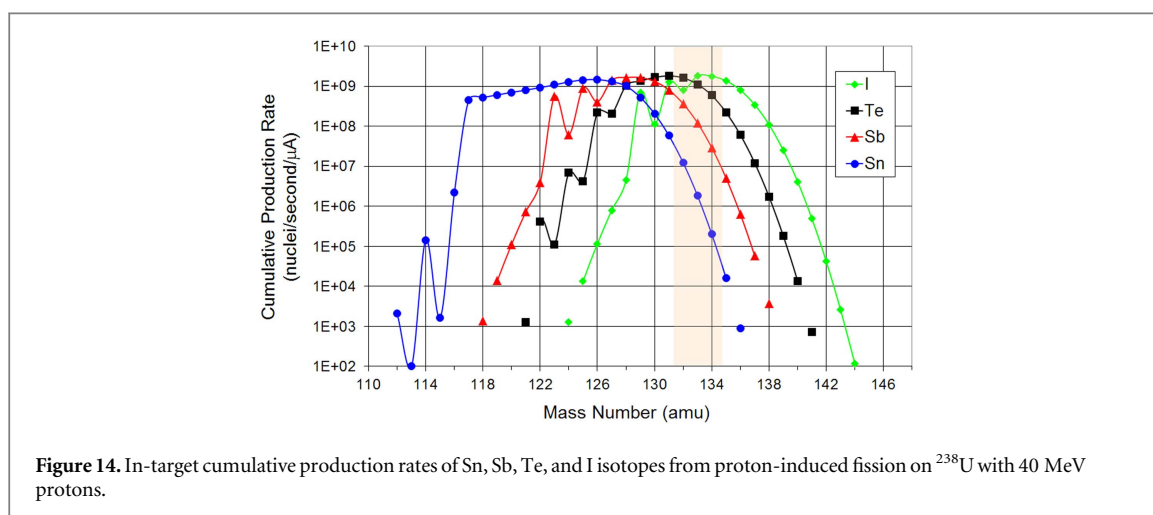

Figure 14. In-target cumulative production rates of Sn, Sb, Te, and I isotopes from proton-induced fission on ^{238}U with 40 MeV protons.

5. Beam purification with negative ions

Beam purity is critical for most experiments with exotic RIBs. Often the beams extracted from an ISOL-type target are contaminated with isobars that have very small mass differences and are usually in quantities exceeding the beams of interest by orders of magnitudes. Consequently, isobar suppression is one of the main challenges for forefront nuclear research on exotic nuclei. A variety of beam purification techniques have been developed including development of ion sources that have high selectivity, such as surface ionization and resonance laser ionization, and using chemical properties to select a particular element. One of the more effective beam purification techniques is based on molecular ion extraction [80] which takes advantage of differences in the chemistry of neighboring elements resulting in different efficiencies to form molecular ions at high temperatures. At the HRIBF, this technique was successfully utilized by extracting the positively charged molecular ions, selecting the mass in the first-stage mass separator, and passing the beam through the Cs-vapor charge exchange cell to break up the molecule and to generate the negatively charged atomic ions, which were then injected into the tandem for post-acceleration. A good example of this technique used to greatly enhance the quality of the RIB is the purification of Sn and Ge beams [81]. The atomic $A = 132$ beam from proton-induced fission in a UC$_x$ target consisted of 87% Te, 12% Sb, and 1% Sn, as shown in figure 14, and the Sn isotope was the nucleus of interest. It was observed that if the Sn isotopes were extracted from the ion source as SnS$^+$ molecular beams, the intensity of the TeS$^+$ and SbS$^+$ beams were at least four orders of magnitude lower. The SnS$^+$ beam was converted to a Sn$^-$ beam in the CEC with an efficiency of about 40%. The resulting negative-ion beams at mass 132 consisted of more than 95% ^{132}Sn$^-$. Beams of ^{132}Sn, purified to ~95% were accelerated to a few MeV/nucleon and delivered to experiments at rates up to 10^6 ions s^{-1}.
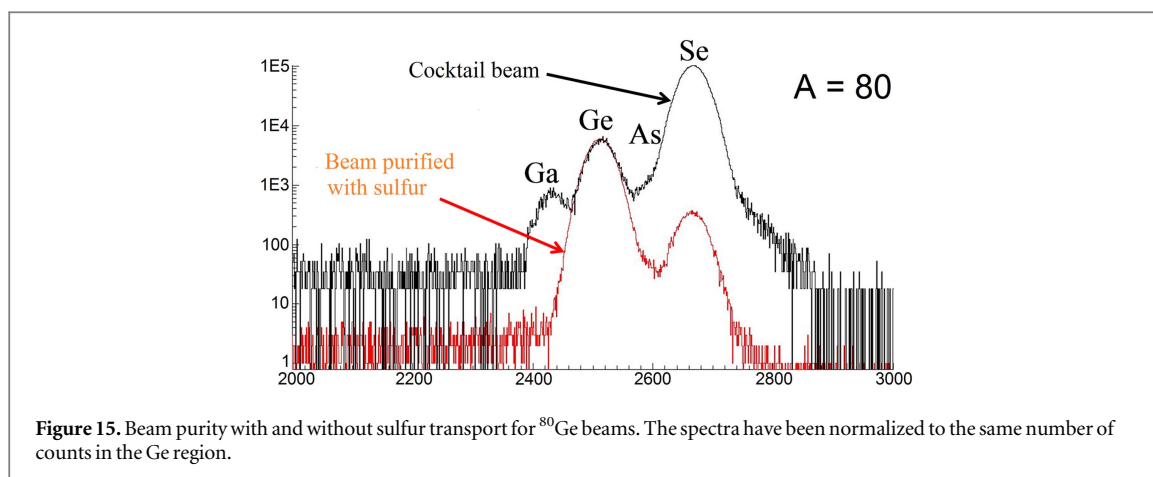
Figure 15. Beam purity with and without sulfur transport for ^{80}Ge beams. The spectra have been normalized to the same number of counts in the Ge region.

Table 5. Accelerated neutron-rich Ge and Sn RIBs at HRIBF, which were purified using sulfide molecular transport followed by molecular breakup in the Cs-vapor charge exchange cell.

RIB species	Half-life	Energy range (MeV)	Highest intensity (pps on target)	Purity (%)	Comments
^{75g}Ge	1.38 h		2×10^5		Purified Ge beams are extracted from the ion source as GeS$^+$
^{77g}Ge	11.2 h		8×10^5		
^{78}Ge	1.47 h	175	2×10^6	67	
^{79g}Ge	19 s		2×10^5		
^{80}Ge	29.5 s	179	2×10^5	95	
^{81}Ge	7.6 s		8×10^4		
^{82}Ge	4.55 s	183–350	3×10^4	22	
^{83}Ge	1.85 s	220–327	1500	43	
^{84}Ge	0.947 s	220–327	95	12	
^{123m}Sn	40.1 m		1×10^7	18	
^{125m}Sn	9.5 m		5×10^6	0.8	
^{126}Sn	2.3×10^5 a	378	1×10^7	50	Purified Sn beams are extracted from the ion source as SnS$^+$
^{127g}Sn	2.12 h		1×10^7		
^{128g}Sn	59.1 m	384	3×10^6	>99	
^{129m}Sn	6.9 m		5×10^5		
^{130}Sn	3.72 m	391	3×10^6	>99	
^{131}Sn	58.4 s		2×10^6		
^{132}Sn	39.7 s	316–560	9×10^5	96	
^{133}Sn	1.44 s	316	2×10^4	33	
^{134}Sn	1.04 s	316–560	3×10^3	38	

Similarly, the negative-ion beams of Ge isotopes were strongly contaminated with isotopes of Ga, As, and Se when they were extracted from the ion source as atomic ions but were about 95% pure when extracted as GeS$^+$ ions, as illustrated in figure 15.

In general, the molecular transport and breakup method resulted in a net relative enhancement of the negative ion of group IVA species (Sn$^-$ or Ge$^-$) by a factor of $\sim 10^4$ relative to neighboring isobaric contaminant species (Sb$^-$ and Te$^-$, or As$^-$ and Se$^-$). Table 5 presents the post-accelerated neutron-rich Ge and Sn RIBs at HRIBF with enhanced purity using sulfide extraction. The production of sulfide molecules was achieved by introducing H$_2$S gas into the target enclosure during bombardment in a controlled manner using a variable leak. Other molecules used to enhance beam purity include chlorides for Ga and In beams and fluorides for Sr and Ba beams [82].

6. Future

We have reported the present status of the development and operation of negative-ion sources used to produce RIBs. At both HRIBF and ISOLDE, these developments lead to the production of a range of specific, yet very important, negatively charged RIBs. The purity of these beams was unmatched. The specificities of the elements

for which they are best suited, namely halogens and a few other possible beams, calls for further developments to further improve the results, for instance on the compatibility of the sources with different production targets or to improve the release characteristics to reach more exotic beams. This could possibly be achieved using new types of low work function materials, new materials to reduce the adsorption times of the halogens, as well as more favorable geometries to further increase the ionization efficiency for the most challenging of the halogens, Astatine.

Another future development will need to be focused on the post-acceleration of negative RIBs at facilities such as ISOLDE or TRIUMF, where the negative ions need to be converted to positive-ions before re-acceleration. Charge-breeding using an electron beam ion source or an electron cyclotron resonance ion source has been widely used [83] to convert singly charged positive ions into highly charged positive ions for subsequent acceleration. It may be possible to utilize such charge-breeding techniques to convert negatively charged atomic or molecular RIBs for post-acceleration, but to our knowledge, no attempts of charge breeding starting from negative-ion beams have yet been undertaken. The challenge will be to efficiently capture the negative ions and at the same time effectively extract the highly charged positive ions. New and novel injection schemes will be needed.

Acknowledgments

ORCID iDs

Y Liu ⓘ https://orcid.org/0000-0001-5903-3112

References

[1] NSAC 2015 *Reaching for the Horizon: The 2015 Long Range Plan for Nuclear Science* https://science.energy.gov/np/nsac/
[2] Gelletly W 2001 *Proc. Am. Phil. Soc.* **145** 519–54
[3] National Research Council 2007 *Scientific Opportunities with a Rare-Isotope Facility in the United States* (Washington, DC: The National Academies Press) (https://doi.org/10.17226/11796)
[4] Blumenfeld Y, Nilsson T and Van Duppen P 2013 *Phys. Scr.* **T152** 014023
[5] Nilsson T 2013 *Nucl. Instrum. Methods* B **317** 194–200
[6] Balantekin A B *et al* 2014 *Mod. Phys. Lett.* A **29** 1430010
[7] Morrissey D J and Sherrill B M 2004 In-flight separation of projectile fragments *The Euroschool Lectures on Physics with Exotic Beams Vol I* (*Lecture Notes in Physics* vol 651) ed J S Al-Khalili and E Roeckl (Berlin: Springer) p 113
[8] Ravn H L 1998 *Phil. Trans. R. Soc.* A **356** 1955–84
[9] Van Duppen P 2006 Isotope separation on line and post acceleration *The Euroschool Lectures on Physics with Exotic Beams Vol II* (*Lecture Notes in Physics* vol 700) ed J S Al-Khalili and E Roeckl (Berlin: Springer) p 37
[10] Herlert A 2010 *Nucl. Phys. News* **20** 5–12
[11] Dilling J, Kruecken R and Merminga L 2014 ISAC and ARIEL: the TRIUMF radioactive beam facilities and the scientific program *Hyperfine Interact.* **225** 1–284
[12] Beene J R, Bardayan D W, Galindo-Uribarri A, Gross C J, Jones K L, Liang J F, Nazarewicz W, Stracener D W, Tatum B A and Varner R L 2011 *J. Phys. G: Nucl. Part. Phys.* **38** 024002
[13] de Angelis G *et al* 2016 *EPJ Web Conf.* **107** 01001
[14] Ravn H L 1979 *Phys. Rep.* **54** 201–59
[15] Stora T 2012 *Radioactive Ion Sources* CERN-2013-007 pp 331–49 (http://cds.cern.ch/record/1693046) (accessed: November 2016)
[16] Smith M S and Rehm K E 2001 *Annu. Rev. Nucl. Part. Sci.* **51** 91–130
[17] Venezia A and Amiel S 1970 *Nucl. Instrum. Methods* **87** 307–9
[18] Shmid M, Engler G and Yoresh I 1981 *Nucl. Instrum. Methods* **186** 349–51
[19] Engler G and Rapaport M S 1983 *Z. Phys.* A **314** 59–61
[20] Reeder P L, Wright J F and Alquist L J 1977 *Phys. Rev.* C **15** 2108–18
[21] Stoffels J J 1974 *Nucl. Instrum. Methods* **119** 251–4
[22] Vosicki B, Björnstad T, Carraz L C, Heinemeyer J and Ravn H L 1981 *Nucl. Instrum. Methods* **186** 307–13
[23] Ekstrom C and Robertson L 1980 *Phys. Scr.* **22** 344–7
[24] Ewan G T, Hoff P, Jonson B, Kratz K-L, Larsson P O, Nyman G, Ravn H L and Ziegert W 1984 *Z. Phys.* A **318** 309–14
[25] Rabbel V, Stoehlker U, Muenzel J, Wollnik H, Bloennigen F, Kobras K and Lippert W 1987 *Nucl. Instrum. Methods* B **26** 246–8
[26] Menna M, Catherall R, Lettry J, Noah E and Stora T (The ISOLDE collaboration) 2008 *Nucl. Instrum. Methods* B **266** 4391–3
[27] Alton G D 2005 Negative-ion formation and processes and sources *Electrostatic Accelerators: Fundamentals and Applications* ed R Hellborg (Heidelberg: Springer) pp 223–73
[28] Heinemeier J and Tykesson P 1977 *Rev. Phys. Appl.* **12** 1471–5
[29] Heinemeier J and Hvelplund P 1978 *Nucl. Instrum. Methods* **148** 65–75
     Heinemeier J and Hvelplund P 1978 *Nucl. Instrum. Methods* **148** 425–9
[30] Schlachter A S 1984 *AIP Conf. Proc.* **111** 300–11
[31] Re M, Cuttone G, Celona L, Chines F, Messina E, Rizzo D, Tudisco F and Scuderi V 2007 *Eur. Phys. J. Spec. Top.* **150** 303–6

[32] Ionov N I 1972 *Progress in Surface Science, Part 3* vol 1 (Oxford: Pergamon) pp 237–354

[33] Kawano H and Page F M 1983 *Int. J. Mass Spectrom. Ion Phys.* **50** 1–33

[34] Alton G D 1983 *Applied Atomic Collision Physics, Vol 4: Condensed Matter* ed S Datz (New York: Academic) pp 43–177

[35] Pelletier J, Pomot C and Cocagne J 1979 *J. Appl. Phys.* **50** 4517–23

[36] Chu E and Goebel D M 2012 *IEEE Trans. Plasma Sci.* **40** 2133–44

[37] Alton G D and Mills G D 1996 *Nucl. Instrum. Methods* A **382** 232–6

[38] Kirchner R 1990 *Nucl. Instrum. Methods* A **292** 203–8

[39] Borschevsky A, Pašteka L F, Pershina V, Eliav E and Kaldor U 2015 *Phys. Rev.* A **91** 020501(R)

[40] Schwellnus F *et al* 2009 *Nucl. Instrum. Methods* B **267** 1856–61

[41] Wucher A 2008 *Appl. Surf. Sci.* **255** 1194–200

[42] Yu M L 1981 *Phys. Rev.* B **24** 1147–50

[43] Lang N D 1983 *Phys. Rev.* B **27** 2019–29

[44] Yu M L and Lang N D 1986 *Nucl. Instrum. Methods* B **14** 403–13

[45] Alton G D 1989 *Nucl. Instrum. Methods* B **40/41** 302–7

[46] Maier R, Korschinek G, Spolaore P and Kutschera W 1978 *Nucl. Instrum. Methods* **155** 55–60

[47] Campajola L *et al* 1996 *Z. Phys.* A **356** 107

[48] Roberts A D *et al* 1995 *Nucl. Instrum. Methods* B **103** 523

[49] Rehm K E *et al* 1997 *Nucl. Phys.* A **616** 115c–22c

[50] Rehm K E *et al* 2000 *Nucl. Instrum. Methods* A **449** 208–16

[51] Sonzogni A A *et al* 2000 *Phys. Rev. Lett.* **84** 1651–4

[52] Alton G D, Cui B, Bao Y, Reed C A, Ball J A and Williams C 1999 *AIP Conf. Proc.* **473** 352–9

[53] Liu Y, Cole J M, Reed C A, Williams C L and Alton G D 2003 *AIP Conf. Proc.* **680** 1017–21

[54] Alton G D, Liu Y, Williams C and Murray S N 2000 *Nucl. Instrum. Methods* B **170** 515–22

[55] Welton R F (The HRIBF staff) 2002 *Nucl. Phys.* A **701** 452c–60c

[56] https://phy.ornl.gov/leribss/

[57] Stracener D W, Alton G D, Auble R L, Beene J R, Mueller P E and Bilheux J C 2004 *Nucl. Instrum. Methods* A **521** 126–35

[58] Sundell S and Ravn H (The ISOLDE Collaboration) 1992 *Nucl. Instrum. Methods* B **70** 160–4

[59] Carter H K, Kormicki J, Stracener D W, Breitenbach J B, Blackman J C, Smith M S and Bardayan D W 1997 *Nucl. Instrum. Methods* B **126** 166–9

[60] Alton G D, Welton R F, Cui B, Murray S N and Mills G D 1998 *Nucl. Instrum. Methods* B **142** 578–91

[61] Alton G D, Liu Y, Zaim H and Murray S N 2003 *Nucl. Instrum. Methods* B **211** 425–35

[62] Alton G D, Haynes D L, Mills G D and Olsen D K 1994 *Rev. Sci. Instrum.* **65** 2012–8

[63] Alton G D, Welton R F, Williams S, Cui B and Murray S N 1998 *Rev. Sci. Instrum.* **69** 2313–9

[64] Alton G D, Welton R F, Murray S N and Cui B 1998 *Rev. Sci. Instrum.* **69** 1327–31

[65] Alton G D, Liu Y, Williams C and Murray S N 1999 *AIP Conf. Proc.* **473** 330–40

[66] Bardayan D W 2006 *Eur. Phys. J.* A **27** 97–106

[67] Liang J F 2002 *Acta Phys. Hung. New Ser. Heavy Ion Phys.* **16** 213–21

[68] http://outotec.com/en/Products–services/HSC-Chemistry/

[69] Alton G D, Liu Y and Stracener D W 2006 *Rev. Sci. Instrum.* **77** 03A711

[70] Lettry J *et al* 1997 *Nucl. Instrum. Methods* B **126** 130–4

[71] Turrión M *et al* 2008 *Nucl. Instrum. Methods* B **266** 4674–7

[72] Jones R G 1988 *Prog. Surf. Sci.* **27** 25–160

[73] Perajarvi K *et al* 2003 *Nucl. Instrum. Methods* B **204** 272–7

[74] Pelletier J and Promot C 1979 *Appl. Phys. Lett.* **34** 249–51

[75] Alton G D, Mills G D and Dellwo J 1994 *Rev. Sci. Instrum.* **65** 2006–11

[76] Fitzgerald R 2005 *PhD Thesis* University of North Carolina at Chapel Hill

[77] Middleton R 1989 *A Negative Ion Cookbook* http://tvdg10.phy.bnl.gov/COOKBook/

[78] Alton G D 1976 *IEEE Trans. Nucl. Sci.* **NS-23** 1113–7

[79] Gross C J *et al* 2012 *Phys. Rev.* C **85** 024319

[80] Kirchner R 2003 *Nucl. Instrum. Methods* B **204** 179–90

[81] Stracener D W 2003 *Nucl. Instrum. Methods* B **204** 42–7

[82] Ravn H L, Sundell S and Westgaard L 1975 *Nucl. Instrum. Methods* **123** 131–44

[83] Wenander F J C *CERN Yellow Report* CERN-2013-007 pp 351–80